Coherent Raman spectroscopy of $YBa_2Cu_3O_7$

A. Rubano,[1] D. Paparo,[2] F. Miletto Granozio,[2] U. Scotti di Uccio,[2,3] and L. Marrucci[1,2,*]

[1]*Dipartimento di Scienze Fisiche, Università di Napoli "Federico II", Complesso di Monte S. Angelo, via Cintia, 80126 Napoli, Italy*
[2]*CNR-INFM Coherentia, c/o Dip. di Scienze Fisiche, Università di Napoli, Italy*
[3] *DiMSAT, Università di Cassino, via Di Biase 43, 03043 Cassino (FR), Italy*
[*]*Corresponding author: lorenzo.marrucci@na.infn.it*

Abstract: We report preliminary results on the optical driving and spectroscopic detection of Raman-active features in thin films of the high-temperature superconductor $YBa_2Cu_3O_7$ in its normal phase by means of coherent Stokes and anti-Stokes Raman scattering, in a reflection geometry. Reference measurements on germanium are also reported. We observe phonon resonances which interfere coherently with a broad electronic resonance centered at zero frequency, giving rise to characteristic asymmetric spectral features. Our measurements provide a first step towards applying nonlinear optical wave-mixing spectroscopy to correlated electron systems.

OCIS codes: (190.4380) Nonlinear optics, four-wave mixing; (300.6230) Spectroscopy, coherent anti-Stokes Raman scattering

References and links

1. M. D. Levenson, *Introduction to Nonlinear Laser Spectroscopy* (Academic Press, New York, 1982).
2. Y. R. Shen, *The Principles of Nonlinear Optics* (John Wiley & Sons, New York, 1984).
3. S. Mukamel, *Principles of Nonlinear Optical Spectroscopy* (Oxford University Press, New York, 1995).
4. A. M. Zheltikov, "Coherent anti-Stokes Raman scattering: from proof-of-the-principle experiments to femtosecond CARS and higher order wave-mixing generalizations," J. Raman Spectrosc. **31**, 653–667 (2000).
5. D. S. Chemla and J. Shah, "Many-body and correlation effects in semiconductors," Nature **411**, 549–557 (2001).
6. M. Cardona, "Raman scattering in high T superconductors: phonons, electrons, and electronphonon interaction," Physica C **317-318**, 30–54 (1999).
7. C. Thomsen and G. Kaczmarczyk, "Vibrational Raman spectroscopy of high-temperature superconductors," in *Handbook of vibrational spectroscopy*, J. M. Chalmers and P. R. Griffiths, eds., pp. 2651–2669 (John Wiley & Sons, Chichester, 2002).
8. T. P. Devereaux and R. Hackl, "Inelastic light scattering from correlated electrons," Rev. Mod. Phys. **79**, 175–233 (2007).
9. M. L. Tacon, A. Sacuto, A. Georges, G. Kotliar, Y. Gallais, D. Colson, and A. Forget, "Two energy scales and two distinct quasiparticle dynamics in the superconducting state of the underdoped cuprates," Nature Phys. **2**, 537–543 (2006).
10. D. M. Newns and C. C. Tsuei, "Fluctuating CuOCu bond model of high-temperature superconductivity," Nature Phys. **3**, 184–191 (2007).
11. I. Bozovic, "Plasmons in cuprate superconductors," Phys. Rev. B **42**, 1969–1984 (1990).
12. It must be noted that our experimental geometry leads to a small walk-off of the output CRS wave during wavelength tuning, small enough not to lead to significant variations in our detection sensitivity (to minimize this effect, we arranged the detection line so as to have all beam displacements occurring along the long axis of the monochromator entrance slit).
13. S. E. Inderhees, M. B. Salamon, T. A. Friedmann, and D. M. Ginsberg, "Measurement of the specific-heat anomaly at the superconducting transition of $YBa_2Cu_3O_{7-\delta}$," Phys. Rev. B **36**, 2401–2403 (1987).

#93675 - $15.00 USD Received 10 Mar 2008; revised 24 Apr 2008; accepted 24 Apr 2008; published 4 Jun 2008

14. J. R. Meyer, F. J. Bartoli, E. R. Youngdale, and C. A. Hoffman, "Effects of energy gap and band structure on free-carrier nonlinear susceptibilites in semiconductors," J. Appl. Phys. **70**, 4317–4321 (1991).
15. B. Fainberg, "Laser-induced grating spectroscopy of electron-phonon interaction in metallic and high-temperature superconductors," Opt. Commun. **89**, 403–409 (1992).
16. V. N. Bagratashvili, V. A. Lobastov, A. N. Zherikhin, V. M. Petnikova, and V. V. Shuvalov, "Nonlinear spectroscopy of Y-Ba-Cu-O and Ni thin films by a biharmonic pumping technique," Phys. Lett. A **164**, 99–102 (1992).
17. A. N. Zherikhin, V. A. Lobastov, V. M. Petnikova, and V. V. Shuvalov, "Biharmonic pumping technique for Y-Ba-Cu-O energy spectrum research in the vicinity of the phase transition," Phys. Lett. A **179**, 145–148 (1993).
18. N. Gedik, J. Orenstein, R. Liang, D. A. Bonn, and W. N. Hardy, "Diffusion of nonequilibrium quasi-particles in a cuprate superconductor," Science **300**, 1410– 1412 (2003).

Coherent Raman scattering (CRS) is a well known wave-mixing nonlinear optical process in which two input optical waves having different frequencies and superimposed in a medium drive a material excitation via their beating interference, thus inducing their own frequency-shifted diffraction [1, 2]. In contrast to ordinary (incoherent) linear laser Raman scattering (LRS), in CRS the generated output waves have well-defined propagation directions and frequencies fixed by the input waves, as a result of the coherent nature of the interaction. In particular, coherent Stokes/anti-Stokes Raman scattering (CSRS/CARS) are based on generating and detecting the waves that are, respectively, red-shifted and blue-shifted by a single beat frequency. All these processes are enhanced when the beat frequency approaches the Raman-active resonances in the material, which can therefore be investigated by means of CRS. These spectroscopic techniques, or their several variants and extensions [1, 2], by today form a mature field of technology and are broadly applied to investigating a wide range of materials, including gases, fluids, semiconductors, and even biological tissues [3, 4, 5]. Nevertheless, the application of CRS techniques to high-temperature superconductors (HTS) and other metallic perovskite-like oxides has been very limited, thus far, possibly due to the strong absorption and relatively low optical damage thresholds of these materials. It must be noted that LRS has instead played and still plays a central role in the investigation of these materials, because it allows a rather simple direct probing of their low-energy phononic and electronic resonances [6, 7, 8], with a good sensitivity to the gap and pseudo-gap transitions and even to their underlying symmetry [8, 9]. Since CRS techniques are sensitive to the same degrees of freedom as LRS, and introduce additional options such as time-resolution, selective excitation, phase-sensitive measurements, etc., it is worth trying to extend their application to these fascinating materials as well. These features of CRS might, e.g., prove useful for testing certain new models that have been recently proposed for HTS [10].

Here, we demonstrate the applicability of CRS to the selective excitation and phase-sensitive detection of phonon resonances in metallic $YBa_2Cu_3O_7$ (YBCO) films. In contrast to the more standard applications of CRS, in our experiments we adopted a geometry in which the CRS output radiated *in reflection* is detected and used for our spectroscopic analysis. This makes our technique sensitive to a thickness roughly corresponding to an optical penetration length (60-70 nm for YBCO at our working wavelengths [11]) and applicable to opaque thick films and single crystals. Moreover, our reflection geometry makes the technique independent of three-dimensional phase-matching conditions or substrate contributions that may complicate the interpretation of spectra.

The layout of our experimental setup is shown in Fig. 1a. The optical source is a pulsed Nd:YAG laser emitting pulses of 26 ps of duration full-width-at-half-maximum (FWHM) at a repetition rate of 10 Hz. The second harmonic of this light (at a wavelength of 532.1 nm) is used as one of the two input waves (hereafter called "pump") in the CRS process. The other input (hereafter called "tuner") is obtained from an optical parametric generator (OPG) pumped by the third harmonic of the same laser light, so as to ensure computer-controlled wavelength

#93675 - $15.00 USD Received 10 Mar 2008; revised 24 Apr 2008; accepted 24 Apr 2008; published 4 Jun 2008

tunability in the range 480-680 nm, with a resolution and accuracy of about 10 cm $^{-1}$. The duration of this second pulse was measured to be 21 ps FWHM. Synchronization of the two input pulses is ensured by means of an adjustable optical delay line, and verified by second-harmonic generation in a β-BaB_2O_4 (BBO) nonlinear crystal. The input beams are polarized as desired and weakly focused onto the same spot on the sample, with a waist (half-width at $1/e^2$ of maximum) of 0.73 mm and 1.37 mm for the pump and tuner beams, respectively. Denoting the beat frequency as $\Delta\omega = \omega_p - \omega_t$, where ω_p and ω_t are the pump and tuner frequencies, respectively, the CARS/CSRS output "scattering" frequencies are $\omega_s = \omega_p + \Delta\omega = 2\omega_p - \omega_t$, where $\omega_t < \omega_p$ for CARS, and $\omega_t > \omega_p$ for CSRS. The pump and tuner input wave directions form an angle $\beta_p = 16.85^\circ$ and $\beta_t = 15.15^\circ$, respectively, from the surface normal in a common incidence plane (outside the sample), as shown in Fig. 1b. The corresponding beating interference therefore will form in the sample a moving grating of material excitation lying in the incidence plane. This dynamical grating, in turn, will give rise to a diffracted wave having the CRS frequency ω_s and travelling at an angle $\beta_s \approx 2\beta_p - \beta_t$ within the reflection half-space (more precisely, β_s is fixed by the two-dimensional phase-matching condition for the wave-vector components parallel to the input surface plane). The detection line is precisely aligned along this specific direction [12]. A diaphragm was used for filtering off the other wave-mixing outputs. Additional filtering is provided by a dual-grating monochromator (MC), which is computer controlled so as to be tuned at the CARS/CSRS frequency ω_s for any given tuner frequency ω_t. The signal is then detected by a photomultiplier and amplified by a gated integrator, ensuring further rejection of any stray light. This combination of spatial, wavelength and temporal filtering ensures an almost perfect background suppression except for $\Delta\omega$ below about 50 cm $^{-1}$ (for a monochromator slit of 300 μm), as verified by detecting the signal for blocked pump or tuner light.

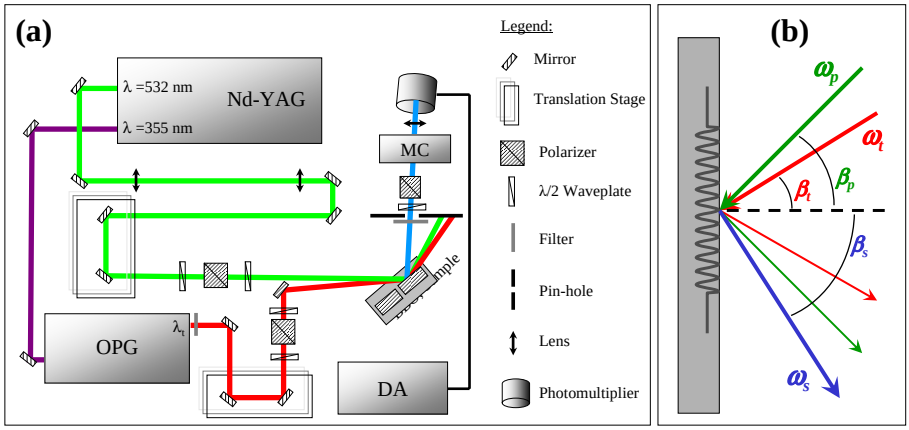

Fig. 1. Experiment illustration. (a) Apparatus layout. Acronym legend: BBO - nonlinear crystal used for synchronization and testing; OPG - optical parametric generator; MC - monochromator; DA - data acquisition. (b) Geometry of the wave mixing process: Shown are the input pump and tuner waves directions (thick green and red arrows), the corresponding reflected waves (thin green and red arrows), and the CRS output wave (thick blue arrow), all lying within the same (incidence) plane. The gray wavy line inside the sample represents the optically-induced dynamical grating.

Our samples are 600 nm thick YBCO twinned thin films grown on MgO substrates, with the $c-$axis normal to the surface, having a critical temperature $T_c = 87$ K. Since we use a reflection geometry and given the shortness of the optical penetration length for the employed

#93675 - $15.00 USD Received 10 Mar 2008; revised 24 Apr 2008; accepted 24 Apr 2008; published 4 Jun 2008

wavelengths (about 60 nm), the substrate contribution to our CRS signal is completely negligible. Typical employed energies per pulse of both the input waves are 50 μJ. All measurements reported in this paper are performed at room temperature, i.e., in the normal metallic phase of YBCO. Taking into account the heat capacity of YBCO [13], reflection losses, and penetration length, we estimate a (space-averaged) laser-induced pulsed heating of 10 K at room temperature. The cumulative heating can be neglected owing to the slow repetition rate. Before YBCO, in order to test the apparatus, we did some CRS measurements on a germanium bulk sample. Moreover, we took reference LRS spectra of both YBCO and germanium samples.

Spectra were acquired for different polarization combinations, probing different nonlinear susceptibility elements $\chi^{(3)}_{ijhk}(-\omega_s;\omega_p,\omega_p,-\omega_t)$. Within a semi-classical model, the latter correspond to the Raman tensor elements R_{ij} according to the law $\chi^{(3)}_{ijhk}\propto R_{ij}R_{hk}+R_{ih}R_{jk}$ [1]. We usually set the polarization of the tuner beam parallel to the analysis polarization of the CRS output, so that for a symmetric Raman tensor our signal was expected to be proportional to R^2_{ij}, with index i corresponding the output/tuner polarization and j to the pump. In particular, we measured the four linear polarization combinations pp, ss, sp and ps, where p (s) labels a polarization lying in the incidence plane (normal to the incidence plane). However, presumably owing to the small incidence angles employed (measured from the surface normal), we actually found that pp and ss ("parallel") polarization combinations always yielded undistinguishable results. The same occurred with ps and sp ("crossed") polarizations.

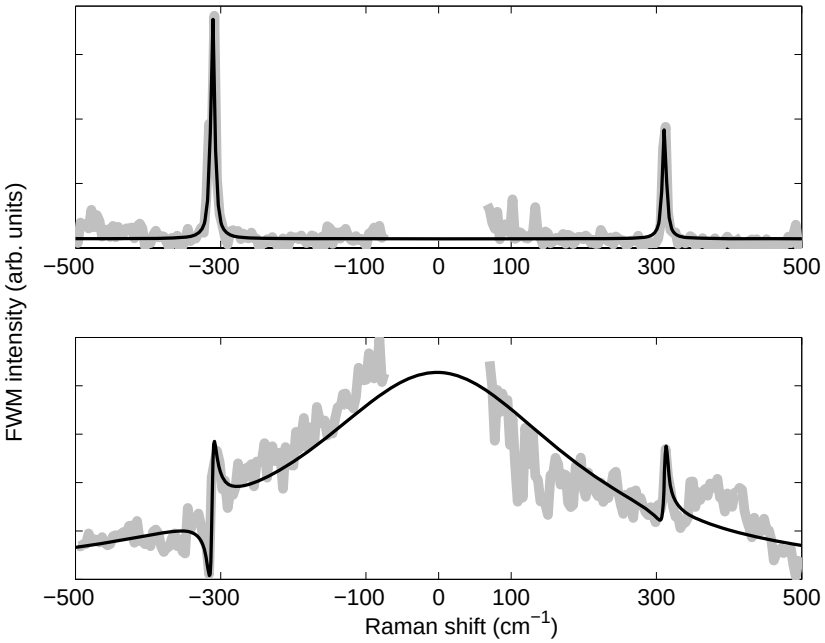

Fig. 2. Coherent Raman reflection spectra from a germanium single crystal. Data: gray lines. Best-fit theory: black line. Upper panel: crossed polarization combination (ps or sp). Lower panel: parallel polarization combination (pp or ss). Positive frequencies refer to the anti-Stokes branch and negative ones to the Stokes branch.

Figure 2 shows the results of our test measurements performed on the germanium sample. Crossed polarization spectra (upper panel) clearly show the optical phonon line of T_{2g} symmetry at $\omega_0 = 310 \pm 10$ cm^{-1}, consistent within our accuracy with the 304 cm^{-1} line seen with LRS. The apparent width of this resonance corresponds to the instrumental spectral resolution.

#93675 - $15.00 USD Received 10 Mar 2008; revised 24 Apr 2008; accepted 24 Apr 2008; published 4 Jun 2008

The same phonon resonance is also visible in the parallel-polarization spectra (lower panel), although here it is superimposed to a broad peak centered at zero frequency, which must be ascribed to an electronic response. This broad feature is of A_{1g} symmetry and we could fit it reasonably well with a Lorentzian function centered at zero frequency and having a width $\Gamma = 230$ cm^{-1}. The broad peak and the phonon line interfere coherently, giving rise to characteristic asymmetric spectral features. These spectra could be fit with the following standard semi-classical expression (for both Stokes and anti-Stokes branches):

$$I(\Delta\omega) = \left| \frac{A}{\Delta\omega + i\Gamma} \mp \frac{B^{(\pm)} e^{i\varphi}}{\Delta\omega \mp \omega_0 + i\gamma_0} \right|^2 \tag{1}$$

where the upper (lower) signs refer to the anti-Stokes (Stokes) branch, i.e., to $\Delta\omega > 0$ ($\Delta\omega < 0$). In using Eq. (1) for fitting the data, the (real) amplitudes A, $B^{(+)}$ and $B^{(-)}$, and the relative phase φ, were adjusted for best-fit. For numerical convergence reasons, the value of φ was varied only in discrete steps of $\pi/12$. If optical losses are negligible, the overall complex amplitudes of the two terms appearing in Eq. (1) should be real, i.e., the phase φ is expected to be either zero or π. Indeed, we find that the choice $\varphi = \pi$ leads to the best fit. Moreover, an adiabatic semiclassical theory of the CRS signal associated with a vibrational resonance predicts that $B^{(+)} = B^{(-)}$. From our best-fit, we obtain instead $B^{(-)} \approx 2B^{(+)}$, but this is to be probably ascribed to an instrumental effect, as our data are not corrected for the varying OPG generation efficiency. We ascribe the broad zero-frequency peak to the free-carrier nonlinearity, including nonparabolicity, thermal-carrier generation and nonequilibrium optical generation contributions [14, 15]. Although we did these measurements mainly as a test of our apparatus, to our knowledge these are the first spectrally-resolved CRS measurements of the germanium optical phonon ever reported.

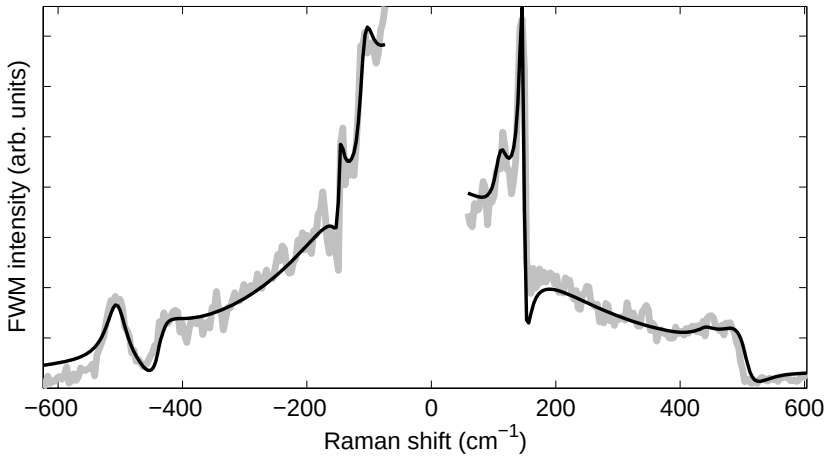

Fig. 3. Coherent Raman reflection spectra from YBCO thin films at room temperature (parallel polarization combination). Data: gray lines. Best-fit theory: black line. Positive frequencies refer to the anti-Stokes branch and negative ones to the Stokes branch.

A typical CRS spectrum of YBCO (for parallel polarizations) is shown in Fig. 3. In this case, spectra acquired with crossed polarizations (not shown) exhibit a vanishingly small signal (independent of the rotation of the sample around its surface normal). Spectra acquired with parallel polarizations, similarly to germanium, exhibit a broad continuum on which narrow spectral features are found at about 110 cm^{-1} and about 150 cm^{-1} on both Stokes and

#93675 - $15.00 USD Received 10 Mar 2008; revised 24 Apr 2008; accepted 24 Apr 2008; published 4 Jun 2008

anti-Stokes branches. These features clearly correspond to the well known Raman-active A_g vibrational modes of Ba and Cu atoms (the latter within the CuO_2 planes) [7]. A relatively narrow spectral feature is also found at about 500 cm^{-1}, more pronounced on the Stokes branch, which can be probably ascribed to the vibration of the oxygen atoms bridging the CuO_2 planes with the CuO chains [7]. A weak feature at 440 cm^{-1} is also probably present in the spectrum on the Stokes branch, which would correspond to one of the vibrational modes of the CuO_2 oxygens [7]. As in germanium, these phonon lines clearly show interference with the continuum. We could fit all the spectra with the following expression, similar to the one used for germanium, but including four phonon lines:

$$I^{(\pm)}(\Delta\omega) = \left| \frac{A^{(\pm)}}{\Delta\omega + i\Gamma^{(\pm)}} \mp \sum_{h=1}^{4} \frac{B_h^{(\pm)} e^{i\varphi_h^{(\pm)}}}{\Delta\omega \mp \omega_h + i\gamma_h} \right|^2 \tag{2}$$

where the index h spans the four phonon lines at the (fixed) frequencies ω_i given in Tab. 1. The best-fit values of the phonon resonance parameters are also given in the table.

Table 1. Best-fit values of the YBCO CRS response parameters entering Eq. (2)

Line #	ω_i (cm^{-1})	γ_i (cm^{-1})	$\varphi_i^{(+)}$ (rad)	$\varphi_i^{(-)}$ (rad)
1	110	12	$\pi/2$	π
2	148	4	$-\pi/3$	$-\pi/3$
3	440	18	$-\pi/3$	$-2\pi/3$
4	505	20	$-\pi/3$	0

In contrast to the case of germanium, here, in order to obtain a quantitative best-fit, we had to assume a different (real) amplitude $A^{(\pm)}$ and width $\Gamma^{(\pm)}$ of the zero-frequency peak for the two Stokes and anti-Stokes branches. This asymmetry may partly be ascribed to instrumental reasons, but a real effect due to the interference with an underlying nonresonant continuum cannot be excluded. From the fit we obtained $\Gamma^{(+)} = 170$ cm^{-1} and $\Gamma^{(-)} = 230$ cm^{-1}. These widths correspond to characteristic electronic relaxation times of the order of 0.2 ps, a reasonable value for electronic free-carrier relaxation, and of the same order of magnitude as previously reported values for YBCO [15].

In conclusion, in this work we demonstrated the feasibility of applying coherent Raman spectroscopies to YBCO in the normal conducting phase, by detecting the spectroscopic signatures of several known Raman-active phonons and their interference with a broad feature ascribed to free-carrier optical excitation. In prospect, we plan to apply our coherent Raman spectroscopy to the electronic coherent behavior arising in the superconducting phase, where only few four-wave mixing experiments have been attempted so far, with puzzling but intriguing findings [16, 17, 18]. The (pulsed) lattice heating induced by our laser system (about 10 K, space-averaged) is already small enough to allow this kind of low-temperature investigation, although a higher repetition-rate lower pulse-energy laser system would of course be advantageous (as long as the cumulative heating remains negligible). A time domain investigation is also foreseen, as some characteristic times of these excitations are expected to be within the reach of our apparatus [18].

#93675 - $15.00 USD Received 10 Mar 2008; revised 24 Apr 2008; accepted 24 Apr 2008; published 4 Jun 2008